International Journal of Microwave and Wireless Technologies

cambridge.org/mrf

A novel dual-band absorber for millimeter-wave RADAR applications

Geethanjali Govindarajan, Mohammed Gulam Nabi Alsath, Kirubaveni Savarimuthu and Malathi Kanagasabai

Department of Electronics and Communication Engineering, College of Engineering Guindy, Anna University, Chennai, 600025 India

Research Paper

Cite this article: Govindarajan G, Gulam Nabi Alsath M, Savarimuthu K, Kanagasabai M (2024) A novel dual-band absorber for millimeter-wave RADAR applications. *International Journal of Microwave and Wireless Technologies*, 1–8. https://doi.org/10.1017/S1759078724001272

Received: 3 January 2024
Revised: 21 November 2024
Accepted: 22 November 2024

Keywords:
absorptivity; ECM; frequency-selective absorber (FSA); stealth; distributed elements; RADAR; bandwidth; Military; metamaterial; dual-band

Corresponding author:
Geethanjali Govindarajan;
Email: geethanjalig5699@gmail.com

Abstract

A linearly polarized dual-resonant millimeter-wave absorber for Radio Detection And Ranging (RADAR) applications is presented in this paper. The frequency-selective absorber (FSA) is composed of solitarily using the distributed elements. The proposed FSA achieves a dual-band resonance characteristic utilizing the mutual coupling between concentric square loops, the second harmonic mode of the Jerusalem cross, and the corrugated cross grids. The proposed dual-band FSA operates from 25.5 to 26.5 GHz (1 GHz) (f_L) and 31.8 GHz–32.5 GHz (0.7 GHz) (f_H) with minimum absorptivity of 96% and 92%, respectively. The desired frequency response of the proposed unit cell is demonstrated by an equivalent circuit model. The FSA prototype is fabricated and the simulated results are validated using experimental measurements. The proposed FSA is a suitable candidate for stealth application in defense and military systems.

Introduction

Stealth technology plays a key role in military warfare. It reduces the visibility of aircraft, ships, and ground missiles in RADAR. RADAR absorbing materials [1–5] are widely used for stealth applications. These absorbers have attracted more consideration due to their low profile, simple fabrication process, and high adaptability in defense applications that require electromagnetic (EM) waves to be absorbed in a specific frequency band. Several researchers have used various techniques [6–12] to design dual-band absorbers for stealth applications. A frequency-selective absorber (FSA) based on a tetra-arrow structure is proposed in reference [13]. The design of an asymmetric dual-arm spiral incorporated with a resistor for stealth technology is detailed in reference [14]. The broadband property of both resonances is obtained by placing the chip resistor in the middle of the unit cell FSA. Multilayer FSAs exploiting the use of lumped elements are described in references [15–17]. Single-layer, wideband microwave absorbers using active elements with 3-dimensional profiles are illustrated in references [18–20]. Multiband absorbers in references [21, 22] are demonstrated by utilizing a large number of resonator structures. The reported absorber is designed in an asymmetric configuration [23] where it offers polarization sensitivity. An absorber for Ka-band sensing applications is designed in reference [24] with a footprint of 0.712 $\lambda_0 \times 0.712\ \lambda_0$, which achieves a minimum absorptivity of 90% with the composition of a higher profile. The dual-frequency response is realized by combining the single resonance, where the f_L and f_H are dependent on each other. To control the resonant frequencies and to improve the impedance performance, the P-type-Intrinsic-N-type (PIN) diodes are incorporated in reference [25] which increases the fabrication complexity. The narrow-band absorbers are designed using octa sharp ship configuration, and modified square ring resonator in references [26, 27], respectively. Dual-band metamaterial absorbers with wide angular stability are reported in references [28, 29]. However, the absorptivity slightly drops at 80% and 85% by increasing the angle of incidence. A high profile of 3 mm is composed in reference [30] to realize the broadband characteristics and to improve the impedance matching. A metamaterial absorber is proposed with a footprint of 1 $\lambda_0 \times 1\ \lambda_0$ in reference [30] for microwave applications. A co-polarized microwave absorber is presented in reference [31]. This absorber is characterized by using a narrow bandwidth, with a minimum absorptivity of 90% at 3.5 and 5.8 GHz. A triple-band absorber is designed using closed loop resonators at reference [32].

The aforementioned methods result in the development of a complex FSA design with a bulkier configuration [30, 31], low absorptivity [24, 30], narrow band [23–33], and polarization sensitivity [23]. In addition, impedance matching using lumped resistors increases the manufacturing difficulty of the FSA. Thus, a low-profile FSA unit cell with desired impedance matching using distributed elements is proposed to reduce the manufacturing complexity with improved performance. A linearly polarized

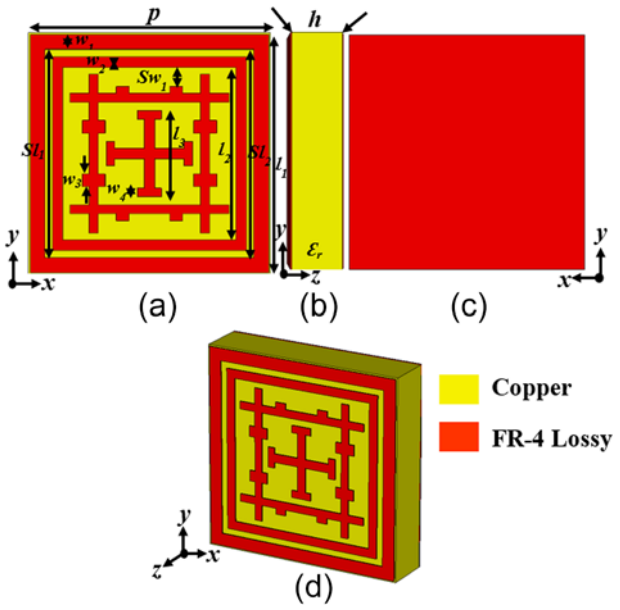

Figure 1. Proposed dual-band absorber. (a) Front view, (b) Side view, (c) Rear view, and (d) Perspective view. $p = 7 \times 7$ mm, $l_1 = 6.95$ mm, $Sl_1 = 6$ mm, $l_2 = 5$ mm, $l_3 = 2$ mm, $Sl_2 = 5.6$ mm, $w_1 = 0.42$ mm, $w_2 = 0.3$ mm, $Sw_1 = 0.5$ mm, $w_3 = 0.2$ mm, $w_4 = 0.25$ mm, $h = 1.6$ mm, $\varepsilon_r = 4.3$ (red: copper, yellow: FR-4 lossy substrate).

dual-wide band FSA in the millimeter-wave (Ka-band) regime exploiting only the distributed elements is presented in this paper. The proposed dual-band absorber achieves a wider absorption band from 25.5 GHz (1 GHz) (f_L), and 31.8–32.5 GHz (0.7 GHz) (f_H) with the minimum absorptivity of 96% and 92% by integrating multiple resonators in a single Printed Circuit Board (PCB) layer. This FSA operates within the RADAR frequency range of 31–32.5 GHz as prescribed by the Federal Communications Commission. Thus, the proposed dual-band absorber can be used for RADAR applications. Further, it can also be used for stealth aspects due to its wider bandwidth properties. The proposed dual-band absorber can be directly implemented in electronic warfare systems. The absorber-loaded systems will not reflect the incident EM waves from the intruders, thereby reducing the RADAR signature and improving the stealth aspects. The organization of the article is as follows: the "Performance analysis of the FSA" section of this paper presents the absorber design, construction, evolution, and analysis. The simulated and measured results of the proposed dual-band FSA are discussed in the "Fabrication and measurement" section followed by conclusions in the "Conclusion" section.

FSA realization

Dual-band millimeter-wave absorber design

The geometry of the proposed FSA is depicted in Fig. 1. The unit cell achieves dual-band resonance characteristics by tightly packing multiple resonant structures as described in Fig. 1(a). Figure 1(b–d) represent the side, rear, and perspective views of the proposed FSA unit cell, respectively. The FSA is developed on a FR-4 substrate ($\varepsilon_r = 4.3$, $\tan\delta = 0.023$ and $h = 1.6$ mm). The proposed dual-band absorber is constructed by utilizing distributed elements to achieve desired impedance matching without the use of additional lumped elements as in references [14–16, 34].

The evolution of the proposed absorber is shown in Fig. 2. The unit cell of the FSA has evolved from a concentric square loop resonator enclosing a Jerusalem cross resonator as illustrated in Fig. 2(a) and (b). The Jerusalem cross is widely used for realizing higher absorptivity characteristics [8, 9] and it is adopted in this research to improve bandwidth and absorptivity performance. The reported combination in Fig. 2(b) offers 800 and 250 MHz bandwidth with a peak absorptivity of 94% and 95%, and reflectance of 32% and 25% at f_L and f_H, respectively. The bandwidth at f_H is limited by the capacitance effect. Hence, a suitable impedance compensation network is required. To accomplish this, an inductive cross grid is introduced as shown in Fig. 2(c). However, the absorptivity is as low as 75%, and reflectance is 28% at f_H. In order to improve the absorptivity and bandwidth performance, the inductance is increased by adding the corrugations to the cross grid as shown in Fig. 2(d). Thus, the proposed absorber achieves the minimum absorptivity of 92% with the reflectance of 15%, and 27% at f_L and f_H, respectively. The wavelength equation is used to optimize the resonant parameters of the proposed absorber. It is inferred in Fig. 3(a), that the absorptivity of the single-layered millimeter-wave absorber is achieved by an optimized inductive element in the appropriate position. Hence, the impedance is matched to obtain a −10 dB reflection coefficient.

Equivalent circuit model

The approximate equivalent circuit model (ECM) of the FSA is shown in Fig. 4(a). The metallic loops, corrugated cross grid, and Jerusalem cross are equivalent to a series LC circuit [9]. In the equivalent circuit of the proposed absorber, "z_{Sub}" is the impedance offered by the dielectric with a thickness of 1.6 mm. Thus, the dielectric impedance "z_{Sub}" is given by [27],

$$Z_{Sub} = \frac{Z_0}{\sqrt{\varepsilon_r}} \tan(\beta h) \tag{1}$$

In the equation, β is the propagation constant, Z_0 is the characteristic impedance and h is the profile. Z_{FSS} is the impedance of the proposed absorber. The effective inductance and capacitance of the square loop are represented as "L_1, L_2" and "C_1, C_2." Similarly, the Jerusalem cross and corrugated cross grid resonators are described as "L_3, C_3" and "L_4, C_4." CC_1 and CC_2 are modelled as coupling capacitors. Model *CC* represents the gap between the unit cells and *Cgs* is the value of the substrate. The total input impedance is given by,

$$Z_{in} = Z_{FSS} \,||\, Z_{Sub} \tag{2}$$

The input reflection coefficient "Γ" is given by,

$$\Gamma = \frac{(Z_{in} - Z_0)}{(Z_{in} + Z_0)} \tag{3}$$

To optimize the absorption of an incident EM wave, it's essential to ensure that the real part of the impedance of the absorber closely matches the characteristic impedance of free space, which is approximately 377 Ω and its imaginary part should be zero for minimum reflection which results in the maximum absorption. The free space impedance is given by,

$$Z_0 = \sqrt{\mu_0/\varepsilon_0} \tag{4}$$

Therefore, the absorption of the incident EM wave is maximized by controlling the resonance of μ and ε. This resonant frequency is governed by the equivalent capacitance (C) and inductance (L)

https://doi.org/10.1017/S1759078724001272 Published online by Cambridge University Press

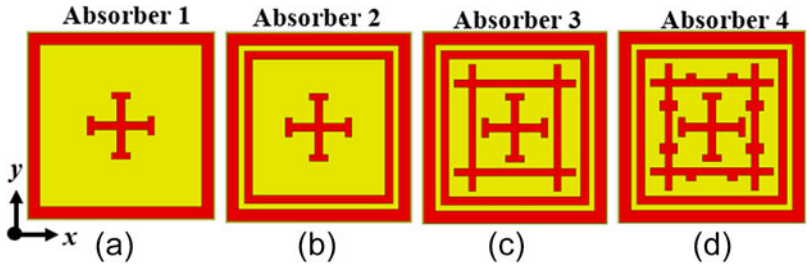

Figure 2. Evolution of the proposed unit cell using Jerusalem cross enclosed within (a) Outer square loop, (b) Outer and inner square loop, (c) Square loops embedded with cross grid, and (d) Square loops with corrugated cross grids.

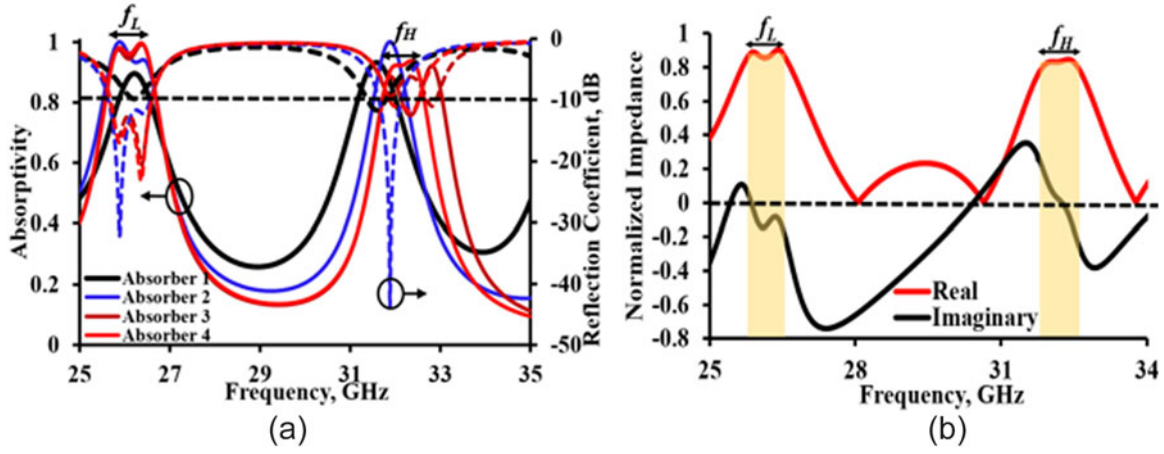

Figure 3. (a) Evolution of the proposed unit cell [solid line: absorptivity, dotted line: reflectance], (b) Normalized impedance of the proposed absorber.

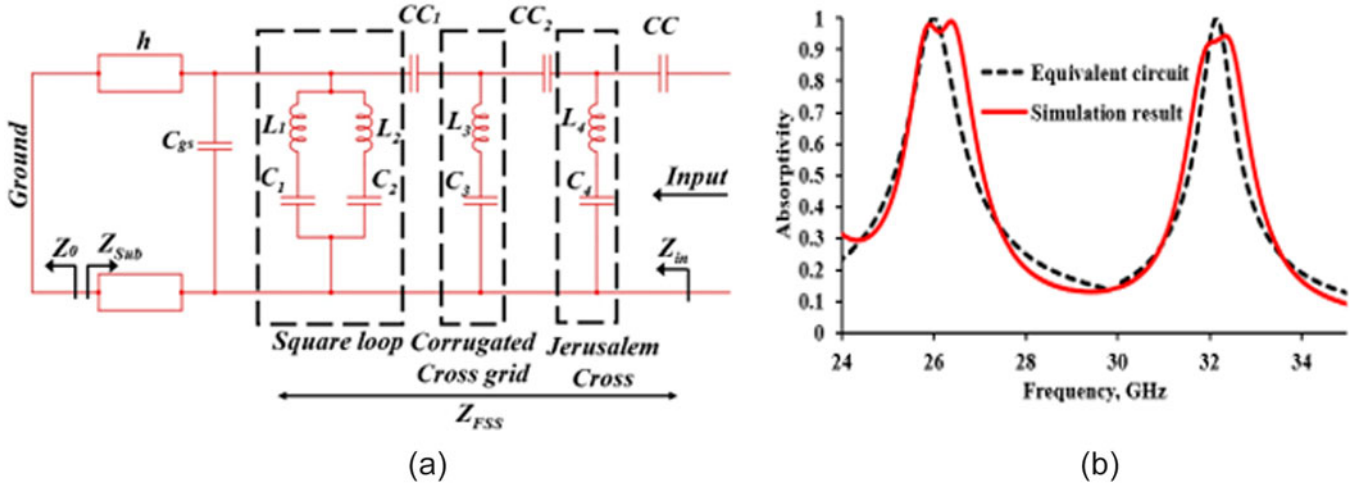

Figure 4. (a) The ECM of the proposed FSA. The approximate value of the circuit parameters Ais *Cgs* (substrate) = 0.408 pF, $L_1 = 0.856$ nH, $C_1 = 0.268$ pF, CC_1 =1.5 pF, $L_2 = 0.534$ nH, C_2 =1.5 pF, CC_2 =1.5 pF, L_3 =0.142 nH, $C_3 = 1.5$ pF, $CC_3 = 1.5$ pF, $L_4 = 0.436$ nH, $C_4 = 0.1$ pF, and $CC = 0.366$ pF, $h = 1.6$ mm, (b) Comparison of the ECM and simulated performance.

of the absorber's metallic structure and metal surface as given by equation (5),

$$\omega_0 = \frac{1}{\sqrt{LC}} \tag{5}$$

When the equivalent series circuit is at resonance, the total reactance, the total reactance of "Z_{FSS}" and "Z_{Sub}" becomes equal and opposite. The component values of the LC resonators are calculated using the model explained in reference [21]. The ECM is developed and simulated using Advanced Design System (ADS) . From Fig. 4(b), it is inferred that the ECM simulation results are consistent with the layout simulation results in Computer Simulation Technology (CST). This confirms the accuracy of the proposed ECM for the proposed FSA configuration. The normalized impedance of the proposed FSA is shown in Fig. 3(b). The relative impedance (z_r) is calculated using the equation in reference [31],

$$z_r = \pm\sqrt{\frac{(1+S_{11})^2}{(1-S_{11})^2}} \tag{6}$$

It is inferred that, at the dual absorption peak frequencies, the real and imaginary parts of the impedance are close to unity and

https://doi.org/10.1017/S1759078724001272 Published online by Cambridge University Press

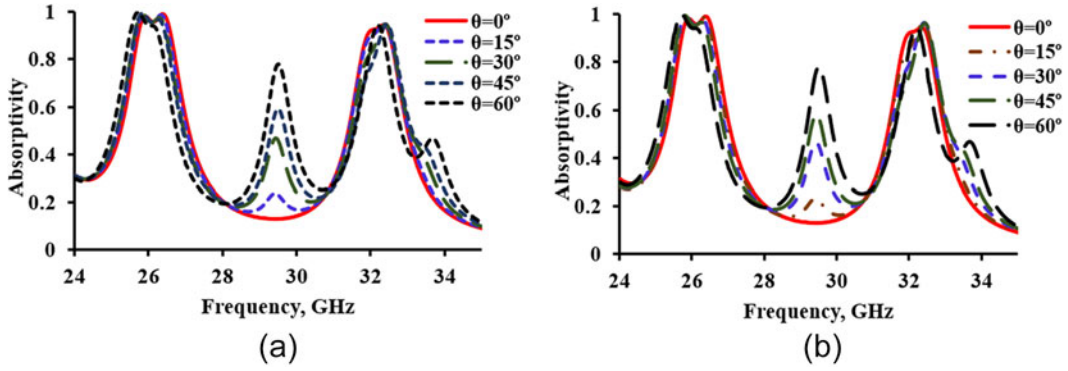

Figure 5. Angular stability (a) TE mode and (b) TM mode.

zero respectively, which validates the perfect impedance matching under free space conditions (377 + j0). Thus, the proposed FSA realizes the minimum reflection and absorptivity close to unity as depicted in Fig. 3(b). The proposed FSA is simulated using CST Microwave Studio 2020. The simulation is carried out using a Frequency domain solver in the tetrahedral mesh with the no. of cells per wavelength of 15. Further, the Floquet port with the periodic boundary conditions is used to simulate the proposed FSA.

Performance analysis of the FSA

Angular stability

The absorption spectra of the proposed FSA under TE and TM modes with different incidence angles are shown in Fig. 5(a, b). At higher oblique incidences, parasitic resonance is induced between the two resonant frequencies. This parasitic resonance is attributed to the corner effects of the induced slots and stubs in the FSA. The corner effect deteriorates the magnetic flux between the metallic resonant layers. This deterioration increases when the oblique incidence (θ) increases and leads to an electric resonance predominant and the associated impedance mismatch [22]. Therefore, the reflection coefficient performance changes at a higher frequency, when the angle of incidence increases [35]. Here, the lower absorption depreciates with the minimum absorptivity of 90% when the angle of the incident is increased to 60°. Similarly, the bandwidth is reduced to 0.3 GHz at the frequency range of 32.2–32.5 GHz with a minimum absorptivity of 85%. Nevertheless, the proposed absorber is stable up to 45° without any bandwidth and absorptivity variations.

The variation of Φ angles at both TE and TM modes is shown in Fig. 6(a, b). It is inferred that, owing to the symmetric structure, the proposed FSA exhibits a stable response with altered bandwidth and absorptivity at f_L and f_H.

Parametric analysis

The effect of the length l_1 of the square loop is plotted in Fig. 7(a). If l_1 is reduced from 6.95 to 6.85 mm, the resonant frequency shifts from 26.0 to 26.7 GHz with declining absorptivity from 90% to 70% at f_L. When the l_1 is increased to 6.98 mm, it produces a narrow bandwidth at f_H with a frequency shift from 25.3 to 26.3 GHz at f_L. Thus, l_1 is optimized and fixed at 6.95 mm. The higher frequency (f_H) is controlled by the width of the stub, w_3. From Fig. 7(b), it is evident that there is a trade-off between the operating bandwidth and absorptivity. With the reasonable reduction in w_3 attains the bandwidth of 0.7 GHz at f_H. When w_3 increases from 0.2 to 0.3 mm the absorptivity reduces from 92% to 75%. Thus, the value of w_3 is optimized to 0.2 mm for the consideration of high absorptivity and desired bandwidth.

Surface current distribution

The surface current distribution of the proposed unit cell at resonant frequencies is shown in Fig. 8. Strong electric current density is induced over the metallic loops and Jerusalem cross at 26 GHz as shown in Fig. 8(a) validating the resonant behavior at f_L. Similarly, at 32 GHz, the corrugated cross grid has more current concentration thus validating the resonant behavior at f_H as shown in Fig. 8(b). Further, it can be inferred that the frequency response of f_L and f_H can be independently controlled in the proposed FSA.

Fabrication and measurement

The proposed FSA is fabricated and tested in the free space using the microwave analyzer. The prototype of the FSA is fabricated using the conventional photolithographic process. The measurement setup of the proposed dual-band FSA is illustrated in Fig. 9(a). The performance of the proposed FSA is measured using a Vector Network Analyzer (VNA), and Transmit/Receive (T/R) horn antennas operating at 18–40 GHz with an aperture dimension of 50 × 50 mm and an average gain of 14 dBi. These antennas are mounted along the line of sight and positioned at a distance of 1 mm $\left(\frac{2D^2}{\lambda}\right)$. The analyzer is calibrated by normalizing the operating frequency range and power level. The measured and simulated results of the dual-band absorber are shown in Fig. 9(b). The inset of Fig. 9(b) depicts an array of 28 × 28 cells fabricated on the FR-4 substrate ($h = 1.6$ mm). The measured bandwidth of 1.5 and 1 GHz with 100% absorptivity is realized at f_L and f_H. The discrepancy between the measured and simulated results at f_L occurs due to the higher losses of the substrate. Table 1 shows the comparison of the proposed FSA with the state-of-the-art.

The research on the development of dual-band millimeter-wave absorbers at the intended RADAR frequency range (31.4–33 GHz) is limited. The higher absorptivity and enhanced bandwidth are highly essential to satisfy the requirements of RADAR or stealth applications [9]. Thus, the work of the proposed absorber is compared with other relevant works (Table 1) with an absorption rate of 90%,

https://doi.org/10.1017/S1759078724001272 Published online by Cambridge University Press

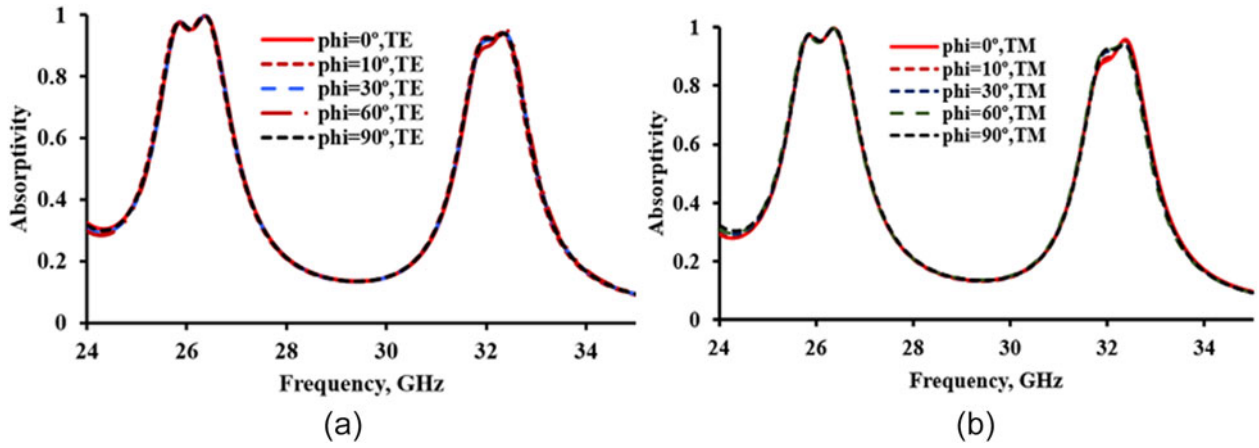

Figure 6. Polarization stability (a) TE mode and (b) TM mode.

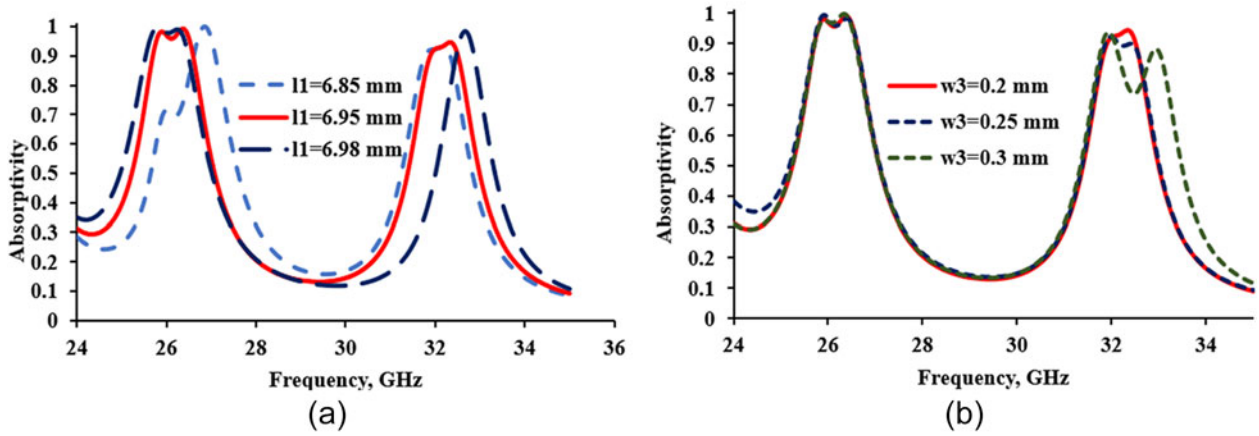

Figure 7. (a) Optimization of the length of the outer square loop (l_1), (b) Optimization of the width of the stub (w_3).

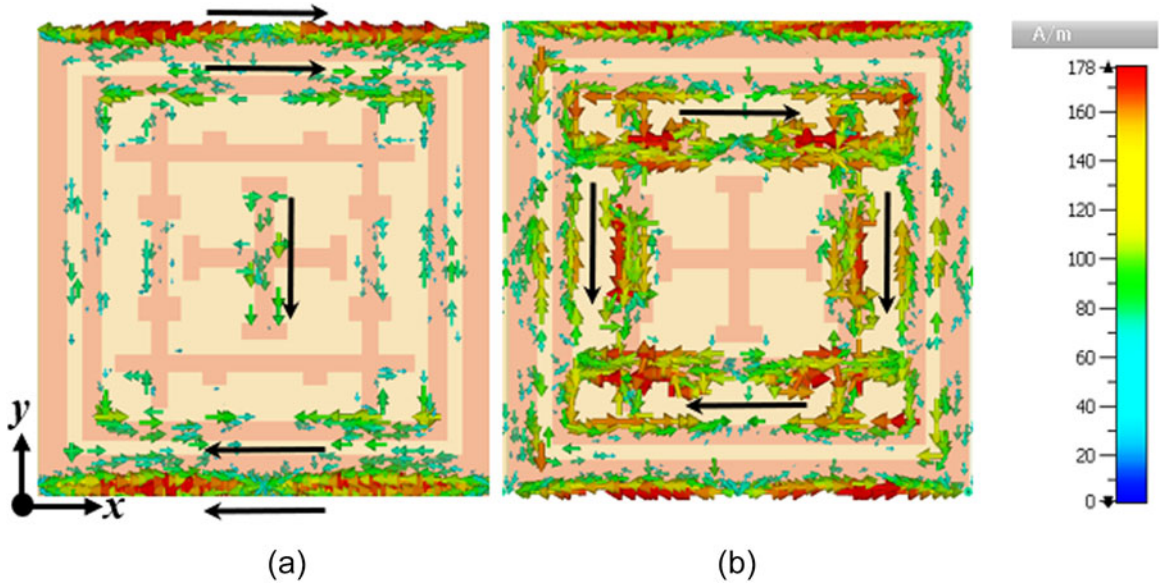

Figure 8. Surface current distribution at contour representation (a) 26 GHz and (b) 32 GHz.

https://doi.org/10.1017/S1759078724001272 Published online by Cambridge University Press

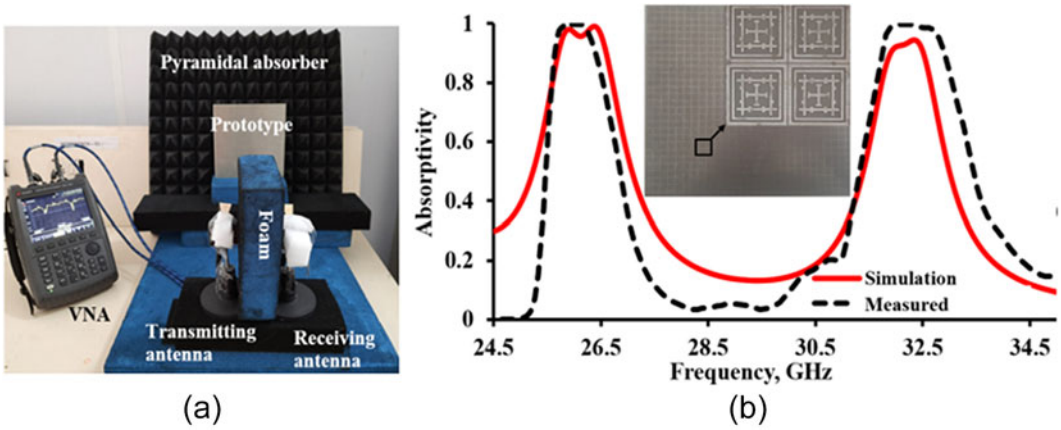

Figure 9. (a) Measurement setup, (b) Absorptivity of the simulated and measured result (inset: fabricated phototype with a magnified view).

Table 1. Quantitative comparison of the proposed absorber with the state-of-art

Ref	UCS($(\lambda_0 \times \lambda_0)$)	Frequency range(GHz)	Techniques used	Bandwidth(GHz)	θ	Absorptivity (%)
[23]	0.17 × 0.56	$f_L = 30.8–31.2^*$	Dirac cone metasurfaces	0.4*	NR	98
[24]	0.71	$f_L = 21.4–21.8 f_H = 23.8–24.4$	Circular split ring resonators	0.4, 0.7	90°	90
[25]	0.17	$f_L = 2.06 f_H = 4.02$	Via and PIN diodes	0.5	60°	92
[26]	0.3*	$f_L = 4.0 f_H = 5.6$	Octa star ship configuration	<0.05	30°	99,97
[27]	0.19	$f_L = 4.19 f_M = 6.64 f_H = 9.95$	Modified double square ring resonator	<0.68	45°	97.5, 96.5,98.8
[28]	0.08	$f_L = 2.45 f_H = 5.61$	Tetra arrow resonator	<0.05	60°	98.8,99.8
[29]	0.43	$f_L = 5.2 f_H = 10.4$	Concentric circular ring	<0.1	60°	98
[33]	NR	$f_L = 5.42 f_H = 12.7–15.0$	Lumped resistors	<0.03*, 2.3	45°	91.7, 90
[30]	1	$f_L = 27.3–27.7 f_H = 29.5–31.2$	High profile	0.3,1.76	30°	90
[31]	0.15	$f_L = 3.5 f_H = 5.8$	High profile	<0.07*	30°	90
[32]	0.12	$f_L = 2.4 f_M = 5.5 f_H = 7.51$	Star shaped structures	<0.05*	52°	>98
This work	**0.52**	$\mathbf{f_L = 25.5–26.5 f_H = 31.8–32.5}$	**Distributed elements**	**1, 0.7**	**45°**	**96–100,92–95**

(UCS-unit cell size, f_L- lower frequency, f_M-middle frequency, f_H-higher frequency, NR-not mentioned, *-approximate values, θ-angular stability).

1) The proposed FSA offers a minimum absorptivity of 92% and bandwidth response of 1 GHz at f_L and 0.7 GHz at f_H which is wider than the bandwidth realized in references [23–33].
2) The unit cell dimension in references [24] and [30] is 20% and 69% large than the proposed design.
3) The proposed unit cell has exploited the distributed elements to realize higher absorptivity with wider bandwidth and to reduce the complexity of the design. This is unlike the research in references [25] and [33], where the active and passive elements are incorporated to achieve the necessary impedance matching and bandwidth broadening.
4) The frequency shift is more than 0.5 and 0.75 GHz in references [26] and [30] for incidence angles 15° and 30°, respectively. Furthermore, the absorptivity drastically decreases (<70%) in references [25–29] and [30] at higher oblique incidences. This is unlike the proposed FSA maintains a stable frequency response and absorptivity of 92% up to 45° in both TE and TM modes.
5) The FSA reported in refrences [24] and [30, 33] has poor band separation with intermediate absorptivity maintained at 50%. However, in the presented research, the absorptivity between both bands is as low as 8%.
6) The reported absorber in refrerence [23] is designed in an asymmetric configuration. Similarly, in reference [33] the spiral resonator is rotated to 90° and combined with the original spiral in an orthotropic position to achieve polarization insensitivity and broadband.
7) A high discrepancy between the measured and simulated result is realized in references [24, 26] and [31, 32], whereas the proposed absorber achieves the measured bandwidth of 1.5 and 1 GHz with 100% absorptivity at f_L and f_H.

Conclusion

A novel design of a dual-band absorber is presented for RADAR applications. The proposed absorber is constructed using integrated elements such as Jerusalem cross, and cross grid with corrugations. It is developed by utilizing distributed elements to achieve desired impedance matching without the use of additional lumped elements, and high profile. The minimum absorptivity of 95% and 92% is achieved in the frequency range of 25.5–26.5 GHz (1 GHz) and 31.8–32.5 GHz (0.7 GHz), respectively. The parametric analysis and the surface current distribution for the bandwidth are analyzed and the results are presented in this work. The simulated results are verified by experimental results and show a good agreement which validates the suitability of the proposed absorber for stealth aspects. In future, the rasorber

https://doi.org/10.1017/S1759078724001272 Published online by Cambridge University Press

will be designed and developed with the composition of bandpass FSS.

Competing interests. There is no conflict of interest in the submission

References

1. **Mouritz AP** (2012) *Polymers for Aerospace Structures - Introduction to Aerospace Materials*. Woodhead Publishing.
2. **P. B Niraj and M, Geetha Priya** (2016) *RADAR and Its Applications* 9(28) International Journal of Computer Technology and Applications. 1–9
3. **Zhekov SS, Mei P, Pedersen GF and Fan W** (2023) Hybrid absorber with dual-band performance and high absorption rate. *IEEE Transactions on Electromagnetic Compatibility* **65**(1), 79–87.
4. **Erkmen F and Ramahi OM** (2021) A scalable, dual-band absorber surface for electromagnetic energy harvesting and wireless power transfer. *IEEE Transactions on Antennas and Propagation* **69**(10), 6982–6987.
5. **Carmo CCM, Batalha RMS, Ribeiro LD and Resende ÚC** (2022) Metamaterial-based broadband absorber design. *IEEE Transactions on Magnetics* **58**(2), 1–5.
6. **Debidas Kundu, Akhilesh, Mohan and Ajay, Chakrabaty** (2016) Single-layer wideband microwave absorber using an array of crossed dipoles. *IEEE Antennas and Wireless Propagation Letters* **15**, 1589–1592.
7. **Govindarajan G, Mohammed GNA, Savarimuthu K and Veeraselvam, A** (2023) Miniaturized electromagnetic absorber for millimeter-wave RADAR systems. *Applied Physics A* **129**, 577.
8. **Landy NI** (2006) Perfect metamaterial absorber. *Physical Review Letters* **100**, 207402.
9. **Munk BA** (2000) *Frequency Selective Surfaces: Theory and Design*. New York: Wiley, 15
10. **Kim YJ, Yoo, YJ, Rhee, JY, Kim, YH, Lee, YP et al.** (2015) Dual broadband metamaterial absorber. *Optics Express* **23**, 3861–3868.
11. **Xiong Han, Hong, Jin-Song, Luo, Chao-Ming and Zhong, Lin-Lin** (2013) An ultrathin and broadband metamaterial absorber using multi-layer structures. *Journal of Applied Physics* **114**(6), 1–4.
12. **Ghosh S, and Srivastava, KV** (2017) An angularly stable dual-band FSS with closely spaced resonances using miniaturized unit cell. *IEEE Microwave and Wireless Components Letters* **27**(3), 218–220.
13. **Munaga P, Gosh, S, Bhattacharyya, S, Chaurasiya, D and Srivastava, KV** (2015) An ultra-thin dual-band polarization-independent metamaterial absorber for EMI/EMC applications. In *9th European Conference on Antennas and Propagation (EuCAP)*, 1–4.
14. **Agrawal Alkesh, Misra, Mukul and Singh, Ashutosh** (2016) A dual broadband metamaterial absorber with concentric continuous and split rings resonator structure. In *IEEE Uttar Pradesh Section International Conference on Electrical, Computer and Electronics Engineering (UPCON)* 15, 597–601.
15. **Zhang B, Jin, C and Shen, Z** (2020) Absorptive frequency-selective reflector based on bent metallic strip embedded with chip-resistor. *IEEE Transactions on Antennas and Propagation* **68**, 5736–5741.
16. **Rashid AK, Shen, Z, Aditya, S et al.** (2018) Wideband microwave absorber based on a two-dimensional periodic array of microstrip lines. *IEEE Transactions on Antennas and Propagation* **58**, 3913–3922.
17. **Hamid S, Karnbach, B, Shakhtour, H, Heberling, D et al.** (2015) Thin multilayer frequency selective surface absorber with wide absorption response. In *Loughborough Antennas & Propagation Conference (LAPC)*, 1–5.
18. **Tennant A, Chambers, B et al.** (2014) A single-layer tunable microwave absorber using an active FSS. *IEEE Microwave and Wireless Components Letters* **14**, 46–47.
19. **Li M, Ying Bai, Y, Zhong Wang, B et al.** (2012) An ultrathin and broadband radar absorber using resistive FSS. *IEEE Antennas and Wireless Propagation Letters* **11**, 748–751.
20. **Omar A, Shen, Zhongxiang et al.** (2017) Double-sided parallel strip line resonator for dual-polarized 3-D frequency-selective structure and absorber. *IEEE Transactions on Microwave Theory and Techniques* **65**, 1–9.
21. **Dong J** (2021) A miniaturized quad-stopband frequency selective surface with convoluted and interdigitated stripe based on equivalent circuit model analysis. *Micromachines* **12**, 1–5.
22. **He-Xiu X** (2012) Triple-band polarization-insensitive wide-angle ultra-miniature metamaterial transmission line absorber. *Physical Review B* **86**, 20510.
23. **Kato Y, Morita S, Shiomi H and Sanada A** (2020) Ultrathin perfect absorbers for normal incident waves using Dirac cone metasurfaces with critical external coupling. *IEEE Microwave and Wireless Components Letters* **30**(4), 383–386.
24. **Hakim ML and Alam T, Almutairi, A, Mansor, MF and Tariqul Islam, M** (2021) Polarization insensitivity characterization of dual-band perfect metamaterial absorber for K band sensing applications. *Scientific Reports* **11**, 17829.
25. **Ghosh S and Srivastava KV** (2017) Polarization-insensitive dual-band switchable absorber with independent switching. *IEEE Antennas and Wireless Propagation Letters* **16**, 1687–1690.
26. **Dincer F, Karaaslan M, Unal E and Sabah C** (2013) Dual-band polarization-independent metamaterial absorber based on omega resonator and octa-star strip configuration. *Progress In Electromagnetics Research* **141**, 219–231.
27. **Singh AK, Abegaonkar MP and Koul SK** (2019) Dual- and triple-band polarization insensitive ultrathin conformal metamaterial absorbers with wide angular stability. *IEEE Transactions on Electromagnetic Compatibility* **61**(3), 878–886.
28. **Bagci F and Medina F** (2016) Design of a dual-band metamaterial absorber in WLAN bands with high stability over incidence angle and polarization. In *2016 10th International Congress on Advanced Electromagnetic Materials in Microwaves and Optics (METAMATERIALS)*. Chania, Greece, 46–48
29. **Chaluvadi M and Rao PH** (2019) Wide-angle and polarization insensitive dual-band metamaterial absorber. In *2019 IEEE 5th Global Electromagnetic Compatibility Conference (GEMCCON)*, Bangalore, India.
30. **Musa et al.** (2021) Dual-band metamaterial absorber for Ka-band satellite application. In *7th International Conference on Space Science and Communication (Icon Space)*, 151–155.
31. **Sen G et al.** (2019) A co-polarized microwave absorber with dual mode resonance based on dual split ring geometry for Wi-MAX and WLAN applications. *Progress in Electromagnetics Research* **86**, 145–152.
32. **Genikala S et al** (2023) Triple band single layer microwave absorber based on closed loop resonator structures with high stability under oblique incidence. *AEU-International Journal of Electronics and Communications* **164**, 154629.
33. **Wu YM et al.** (2018) A dual-band broadband metamaterial absorber with wide-angle absorption and polarization insensitivity. In *International Conference on Microwave and Millimeter Wave Technology (ICMMT)*, 1–3 https://ieeexplore.ieee.org/document/8563501.
34. **Tran et al.** (2019) Creating multiband and broadband metamaterial absorber by multiporous square layer structure. *Plasmonics* **14**, 1587–1592.
35. **Ye Q, Liu Y, Lin H et al.** (2012) Multiband metamaterial absorber made of multi-gap SRRs structure. *Journal of Applied Physics* **17**, 155–160.
36. **Abdulkarim YI et al.** (2022) A review on metamaterial absorbers: Microwave to optical. *Frontiers in Physics* **10**, 893791.
37. **Zhou Y et al** (2015) Wafer-scale metamaterials for polarization-insensitive and dual-band perfect absorber. *Nanoscale* **7** 18914–18917.

Geethanjali Govindarajan received her BE degree from Sri Sairam Institute of Technology, West Tambaram in the year 2020. She received her ME degree from Sri Sivasubramaniya Nadar College of Engineering in the year of 2022. She is currently pursuing her Ph. D. degree at Anna University, Chennai. She is a research scholar in the Department of Electronics and Communication Engineering, College of Engineering Guindy (CEG) Campus, Anna University, Chennai. Her research interests are Metamaterial Absorbers, Frequency Selective Rasorber (FSR) for RADAR and defense applications.

https://doi.org/10.1017/S1759078724001272 Published online by Cambridge University Press

Gulam Nabi Alsath Mohammed received his BE, ME, and Ph.D. degrees from Anna University Chennai in the years 2009, 2012, and 2015, respectively. He is currently serving as an Associate Professor in the Department of Electronics and Communication Engineering, Anna University, Chennai, India. His research interests include Microwave Components and Circuits, Antenna Engineering, Signal integrity Analysis, and Solutions to EMI problems. To his credit, he has 2 US patents and 18 Indian patents. He has published several research articles on antennas and microwave components in leading International Journals. He has also presented and published his research papers in the proceedings of International and National conferences. He is currently serving as an Associate Editor in IET Microwaves Antennas and Propagation and Microwave and Optical Technology Letters.

Kirubaveni Savarimuthu obtained her BE and ME degrees from Anna University, Chennai. She currently serves as an Associate Professor in the Department of Electronics and Communication Engineering, Anna University, Chennai. She has 13 years of teaching and research experience. Her research interests include MEMS and NEMS device design and VLSI design. She is currently involved in the growth of ZnO nanorods for piezoelectric energy harvester and gas sensor applications. She is an active life member of IETE and a senior member of IEEE.

Malathi Kanagasabai completed her Bachelor of Engineering in Electronics and Communication Engineering and Master of Engineering in Microwave and Optical Engineering from Madurai Kamarajar University. She received her PhD on "Analysis of Rectangular Shielded Strip Line Enclosures" from Anna University, Chennai. She currently serves as a Professor in the Department of Electronics and Communication Engineering (ECE), Anna University, Chennai. Her research interests are antennas, UWB microwave components, electromagnetic shielding, and signal integrity analysis in RF-printed circuit boards. She has more than 25 granted patents including two US patents. She has authored more than 130+ research articles in leading international journals and guest edited a special section on THz components for Microwave and Optical Technology Letters.

https://doi.org/10.1017/S1759078724001272 Published online by Cambridge University Press